Anharmonicity effects on the extended x-ray-absorption fine structure: The case of cadmium selenide

G. Dalba, P. Fornasini, R. Grisenti, and D. Pasqualini
Dipartimento di Fisica dell'Università degli Studi di Trento and Istituto Nazionale di Fisica della Materia, I-38050 Povo, Trento, Italy

D. Diop
Département de Physique, Université Cheikh Anta Diop, Dakar, Senegal
and Centro CNR-ITC CEFSA, I-38050 Povo, Trento, Italy

F. Monti
Facoltà di Scienze Matematiche Fisiche e Naturali, Università di Verona, Strada le Grazie, I-37134 Verona, Italy
(Received 20 October 1997; revised manuscript received 1 April 1998)

Extended x-ray absorption fine structure (EXAFS) has been measured at the *K* edge of Se in bulk CdSe in the temperature range from 18 to 300 K. The first four cumulants have been obtained as a function of temperature from a data analysis based on the phase difference and amplitude ratio method, taking the 18-K spectrum as reference. The effective distributions of distances $P(r,\lambda)$ and the corresponding mean force potentials $V(r)$ have been reconstructed from the cumulants. The potentials exhibit a shift of the minimum position as a function of temperature. The temperature dependence of the first cumulant depends on both the shape and position of the anharmonic mean force potential. The thermal expansion measured by EXAFS is larger than the one measured by diffraction; the anharmonicity monitored by EXAFS does not reflect only the crystal anharmonicity, but is enhanced by thermal atomic vibrations normal to the bond direction. The correlation of vibrational motion is different in radial and transverse directions. [S0163-1829(98)02132-8]

I. INTRODUCTION

The standard formula for the analysis of the extended x-ray-absorption fine structure (EXAFS) is based on the one-electron single-scattering harmonic approximation.[1] The inadequacy of the harmonic EXAFS formula to deal with asymmetric distributions of interatomic distances was recognized early.[2–4] Several methods of analysis have been developed to overcome this difficulty. For moderately disordered systems the cumulant method[5,6] is particularly appealing because it summarizes the relevant structural and dynamical information in a few parameters that are easily obtained from the experimental spectra.[7–10] The attention has recently been focused on the relation between EXAFS cumulants and interatomic potentials. The main aim is the search for a more accurate interpretation of the experimental data in terms of the thermodynamical properties of materials, like the thermal expansion and the correlation of atomic vibrational motion.

The EXAFS cumulants have been related to the force constants of an effective potential in classical approximation by Tranquada and Ingalls[7] and by Stern *et al.*[11] Frenkel and Rehr first derived relations between the EXAFS cumulants through a perturbative quantum approach based on a single-bond anharmonic Einstein model.[12] Yokoyama and coworkers extended this approach to calculate and compare with experiment the cumulants of biatomic Br_2 and linear triatomic molecules,[13] Pt octahedrally coordinated complexes[14] and tetrahedral MBr_4 molecules ($M=$C, Si, Ge).[15]

Fujikawa and Miyanaga developed a general expression for the EXAFS Debye-Waller factor in crystal lattices (including third and fourth cumulants) from a first-principles quantum statistical approach,[16] and worked out their model for one-dimensional monoatomic and biatomic chains.[17] They also checked the applicability of the Debye and Einstein approximations for tridimensional systems.[18] However, they did not directly address the topic of thermal expansion, and neglected the possible effect of transverse atomic vibrations in their calculations.

The vibrations normal to the bond direction were explicitly considered by Eisenberger and Brown in the analysis of EXAFS phases in asymmetric systems[2] and by Ishii in a calculation of the EXAFS Debye-Waller factor.[19] However, these effects have not been taken into account in the data analysis until very recently. In addition, no attention has been paid to the difference between correlation in the radial and transverse directions.

In an EXAFS study of β-AgI the distributions of interatomic distances and the corresponding mean force potentials $V(r)$ were reconstructed from cumulants at various temperatures within the classical approximation.[10] The mean force potential exhibited a non-negligible shift of its minimum position when the temperature was varied, while its shape was constant. In addition, the thermal expansion measured in β-AgI by EXAFS was larger than the one measured by x-ray diffraction (XRD). A shift of the minimum position of the effective potential was recently found also for CuBr.[20] Actually, the EXAFS cumulants in crystals are directly related to a mean force pair potential that depends on the dynamics of all the atoms within the crystal, and is then in principle temperature dependent.[21]

The discrepancy in thermal expansion between EXAFS and XRD was attributed in Ref. 10 to the thermal vibrations normal to the bond direction, which increase the average

value of the distribution of distances sampled by EXAFS with respect to the crystallographic distance. Moreover, a large difference was found between the correlations in radial and transverse directions. To our knowledge, this effect had never been previously noticed. Stern has confirmed the conclusions of Ref. 10 starting from a slightly different approach.[22]

In a recent EXAFS study of solid krypton in the temperature range from 24 to 43 K, Yokoyama *et al.* measured the thermal expansion of the first, third, and fourth coordination shells; they obtained good agreement with the XRD results by taking into account the effect of transverse vibrations, and considering the same amount of correlation in the radial and transverse directions.[23]

To enhance the effectiveness of the single-bond approach,[12] Van Hung and Rehr included the interactions between absorber and backscatterer atoms and their immediate neighbors into an effective potential.[24] They obtained a good reproduction of the available experimental cumulants of copper, while their coefficient of thermal expansion is lower than the experimental values.[25]

In view of the progress in the theoretical interpretation of anharmonicity in EXAFS, the availability of a larger amount of reliable experimental data on crystals of different structure and complexity is desirable, to check and compare the different approaches and approximations. The relation between pair potential, crystal potential and EXAFS effective potential, the contribution of transverse vibrations to EXAFS anharmonicity, and the relevance of low-temperature quantum effects deserve particular attention.

In this paper we present a set of temperature-dependent EXAFS measurements at the *K* edge of selenium in *bulk* CdSe and the results of their cumulant analysis. The high quality of experimental data allows one to confirm and strengthen the conclusions drawn from the previous measurements on AgI. The dependence on temperature of the minimum of the potential is very evident; as a consequence, the temperature dependence of the first cumulant is determined not only by the shape asymmetry of the potential, but also by the shift of its minimum position. Moreover, also for CdSe as for β-AgI a much larger thermal expansion is measured by EXAFS than by XRD and a different correlation is found for the radial and transverse vibrations.

Besides its contribution to understanding the mechanism of EXAFS, this work is also intended as a calibration of the EXAFS technique for further studies on CdSe *nanoparticles*. Cadmium selenide nanoparticles embedded in glasses are interesting for their electronic properties, which can be varied from molecular to bulk behavior as a function of the cluster dimensions. The structural and dynamical studies of nanoparticles are complicated by the high ratio between surface and bulk atoms and the corresponding competition between surface and bulk behavior.

Only a few structural studies of CdSe nanoclusters are present in the literature. Bawendi *et al.*[26] made an x-ray diffraction (XRD) study of 35–40 Å capped CdSe nanoclusters with both the zinc blende and wurtzite structure. These authors were able to fit XRD spectra by taking into account the effects of thermal disorder and stacking faults, and found that the wurtzite clusters have a better defined structure than the zinc blende ones. However, the x-ray powder patterns were insensitive to local structural perturbations, including the different possible mechanisms of surface reconstruction and the difference between surface and bulk vibrational properties.

An extensive EXAFS study of CdSe nanoparticles of different sizes has been done by Marcus *et al.*[27,28] The use of different production procedures allowed these authors to distinguish between bulk and surface behavior. For the first coordination shell the interatomic distance and the effect of thermal disorder were similar to those of the bulk compounds. The coordination numbers were consistent with a model of a bulk core with some surface terminations. A discrepancy was, however, found between EXAFS and XRD results: when the cluster size decreases, a contraction of interplanar spacing is monitored by XRD, while no corresponding change in interatomic distance is seen by EXAFS. More recently, EXAFS has been used to monitor semiquantitatively the evolution of CdSe quantum dots in a potassium zinc silicate glass.[29]

All these EXAFS studies were performed within the standard harmonic approximation.[1] However, it is reasonable to expect that anharmonicity plays a non-negligible role in the structure and dynamics of clusters. In particular, the competition between bulk and surface properties should produce a deviation of the distribution of interatomic distances from a Gaussian shape. From this point of view, EXAFS is more sensitive than XRD to the sharp features of the asymmetric distance distributions, since it extends to higher values of transferred momentum.

This paper is organized as follows. A short account of the experimental procedure is given in Sec. II. The analysis of data is summarized in Sec. III. In Sec. IV the results are presented and discussed; the attention is focused on the anharmonic corrections to the mean square relative displacement (MSRD), the reconstruction of the distributions of distances and mean force potentials and the critical evaluation of the thermal expansion measured by EXAFS. Section V is dedicated to the conclusions.

A preliminary short account of this work has been given elsewhere.[30]

II. EXPERIMENTAL DETAILS

The measured sample was prepared by grinding a CdSe monocrystal. X-ray powder diffraction revealed a wurtzite structure. The structural parameters for CdSe in wurtzite structure at room temperature are $a=4.299$ Å, $c=7.010$ Å, and $u=0.37596$ (Ref. 31); they correspond to a slight distortion of the first-shell tetrahedron: one atom is at 2.6355 Å, the other three at 2.6299 Å. This distortion gives rise to an asymmetry in the distribution of distances, but the corresponding value of the third cumulant is several orders of magnitude smaller than the values found by EXAFS analysis and attributed to thermal motion. In the following we will then neglect this slight distortion of the first shell.

To get a homogeneous sample of uniform thickness, as required by x-ray absorption measurements in transmission mode, the powder was dispersed in alcohol and slowly deposited on polytetrafluoroethylene membranes. Three sheets with surface density 18 mg/cm^2 were superimposed to obtain a jump $\Delta(\mu x)\simeq 1$ at the *K* edge of selenium.

Temperature-dependent EXAFS measurements at the K edge of Se (12 658 eV) were made at the beamline D42 of the storage ring DCI at LURE, Orsay, France. Electron energy and maximum stored current were 1.85 GeV and 300 mA, respectively. The monochromator was a channel-cut silicon crystal with (331) reflecting faces.

Absorption spectra were recorded in transmission mode, utilizing two ionization chambers filled with argon as detectors; the gas pressures in the two chambers were adjusted to get comparable signals in the EXAFS region of the spectrum. A temperature range extending from 18 to 300 K was systematically explored by means of a helium gas flow cryostat equipped with an electric heater; the temperature was measured by a thermocouple mounted on the sample holder.

Standard energy calibration was made at the K edge of crystalline germanium (11 103 eV). The average acquisition step in the EXAFS region was 3 eV and the integration time 5 s per step. The energy resolution, determined by the joint effects of lifetime of the excited atomic state, angular divergence of the photon beam and rocking curve of the monochromator, was estimated to be $\Delta E \simeq 3.5$ eV. Two spectra were measured at 18 K, three at 300 K, and one at each of the five intermediate temperatures.

III. DATA ANALYSIS

A large uncompensated glitch was present in all the absorption spectra above 13 600 eV (1000 eV past the edge, corresponding to $k \simeq 15$ Å^{-1}) and could not be satisfactorily removed. The EXAFS signals were then utilized only up to $k=15$ Å^{-1}. The data analysis was carried on within the single scattering and plane wave approximations through the well established method of phase difference and amplitude ratio.[1,5,32]

A straight line best fitting the pre-edge signal was preliminarily subtracted from all the spectra. The values of the photoelectron wave vector k were calculated with respect to an energy origin E_0 set at the maximum of the first derivative of each spectrum. A further refinement of the k scales was made by aligning the edges of all spectra to within 0.1 eV. It was *a posteriori* checked that a mismatch of 0.1 eV in the edge positions of two spectra reflects in a difference of interatomic distance of about 0.001 Å.

The EXAFS function was determined as $\chi(k)=[\mu(k)-\mu_1(k)]/\mu_0(k)$, where $\mu(k)$ was the experimental absorption coefficient, $\mu_1(k)$ a spline polynomial best fitting the average behavior of $\mu(k)$ (Fig. 1) and $\mu_0(k)$ a smooth function with a Victoreen-like slope (equal for all spectra) and absolute values normalized to the experimental absorption jump of each spectrum. The $k\chi(k)$ functions are shown in Fig. 2 for three selected temperatures.

The $k^2\chi(k)$ functions were Fourier transformed in the interval $k=3$–15 Å^{-1}. Two different windows were utilized: a Gaussian window and a 20% Hanning window. The magnitudes of the Fourier transformed signals at 18 and 300 K are compared in Fig. 3. The first-shell contribution to EXAFS was isolated by Fourier backtransforming the corresponding peak. The backtransform ranges are indicated by horizontal bars in Fig. 3; in the case of the Hanning window two different ranges were used, respectively excluding and including the nearest side lobes of the main peak. On the whole, three different procedures of filtering were adopted for each spectrum.

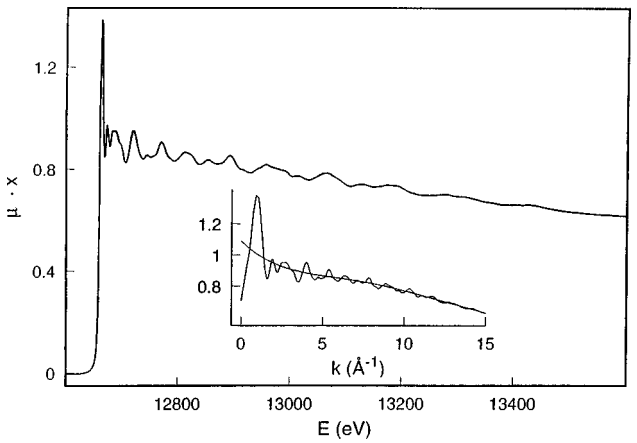

FIG. 1. X-ray-absorption spectrum at the Se K edge of CdSe measured at 18 K. In the inset an enlarged view is plotted as a function of the photoelectron wave vector k together with the polynomial spline best fitting the average behavior of the EXAFS oscillations.

Phases $\Phi(k)$ and amplitudes $A(k)$ of the first-shell EXAFS signals at different temperatures were separately analyzed by the cumulant expansion method truncated at the fourth-order term:

$$\Phi_s(k)-\Phi_r(k)=2k\Delta C_1-(4/3)k^3\Delta C_3, \tag{1a}$$

$$\ln[A_s(k)/A_r(k)]=-2k^2\Delta C_2+(2/3)k^4\Delta C_4. \tag{1b}$$

k is the photoelectron wave vector, s and r refer to signals at $T>18$ K and $T=18$ K, respectively.

At each temperature and for each one of the three procedures of filtering outlined above, the analysis was made using the two different reference spectra measured at 18 K.

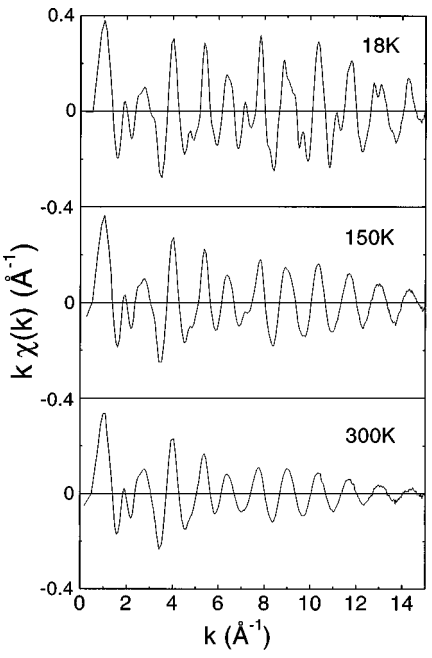

FIG. 2. EXAFS oscillations $k\chi(k)$ at the Se K edge in CdSe at 18, 150, and 300 K.

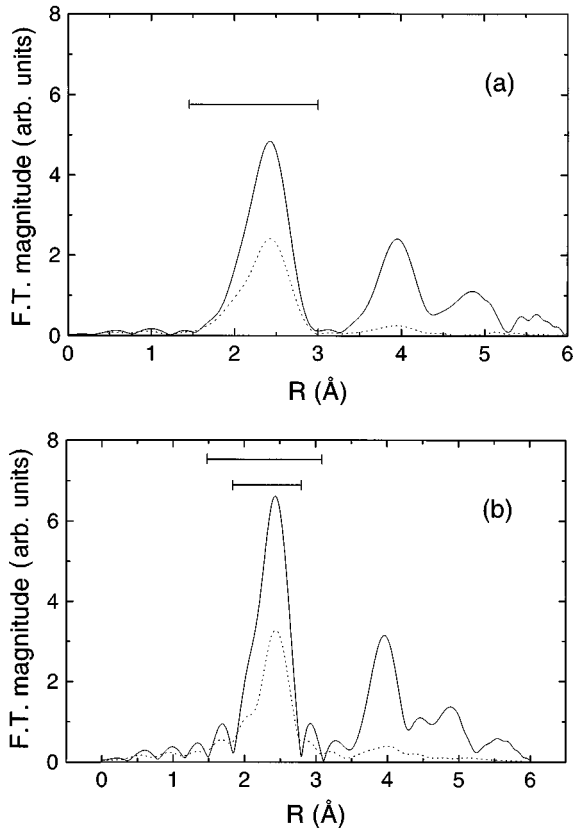

FIG. 3. Magnitudes of the Fourier transforms of the EXAFS signals $k^2\chi(k)$ at 18 K (continuous lines) and 300 K (dashed lines). Two different windows have been used within the k range 3–15 Å^{-1}: Gaussian (a) and 20% Hanning (b). The horizontal bars show the different intervals chosen to backtransform the first-shell contribution.

Typical plots of phase differences and logarithms of amplitude ratios are shown in Fig. 4 together with the best fitting polynomials. The use of a Gaussian window in the Fourier transform procedure produced smoother curves of phase differences and amplitude ratios than a Hanning window including side lobes in the backtransform, but no systematic differences were found in the numerical values of the fitting parameters ΔC_i.

In Fig. 4 the phase difference divided by k and the logarithm of the amplitudes ratio are both plotted against k^2. In this way, in the phase plot the differences of first and third cumulant are proportional to intercept and slope, respectively:[9] the increase of both ΔC_1 and ΔC_3 from 95 to 300 K is immediately evident.

The four polynomial coefficients ΔC_i $(i=1,4)$ obtained from the analysis are shown in Fig. 5 as a function of temperature. The error bars are the standard deviations of the values from the six different analysis procedures utilized (three different Fourier filtering procedures times two 18-K reference spectra). The temperature dependence of the polynomial coefficients is consistent with the first-order behavior expected for thermal cumulants in classical approximation: Einstein-like, parabolic and cubic for ΔC_2, ΔC_3, and ΔC_4, respectively.[7] This suggests that the convergence of the cumulant series is sufficiently fast to guarantee that the first four cumulants describe the EXAFS signal within 15 Å^{-1}

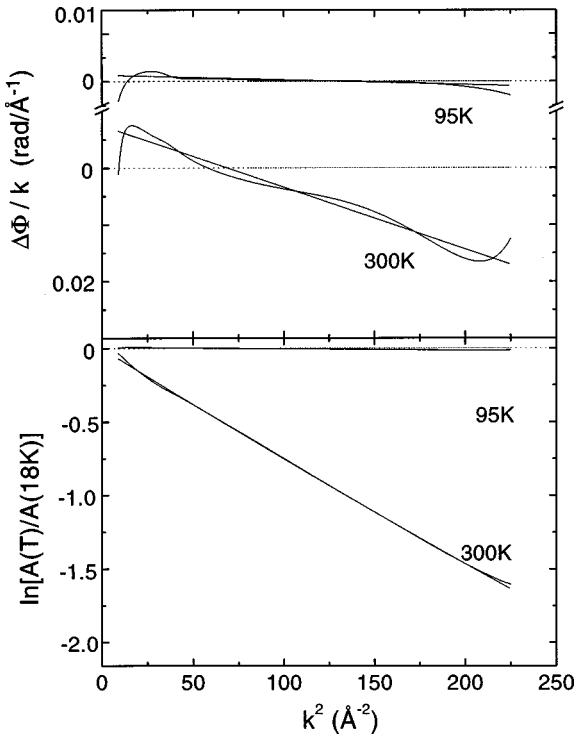

FIG. 4. Phase differences $\Delta\Phi/k$ (top) and logarithms of amplitude ratios (bottom) plotted as a function of k^2 for selected temperatures. The reference is a spectrum measured at 18 K. The phases and amplitudes shown have been obtained after Fourier transforming with a Gaussian window.

up to 300 K; the polynomial coefficients C_i can then be identified with the cumulants of the effective distribution of Se-Cd distances.

In Fig. 5(c) the open triangles are the values ΔC_2 of the second cumulant obtained for a bulk CdSe sample with the zinc blende structure by Marcus *et al.*, taking a spectrum at 8 K as a reference.[27] The analysis of Marcus *et al.* was made

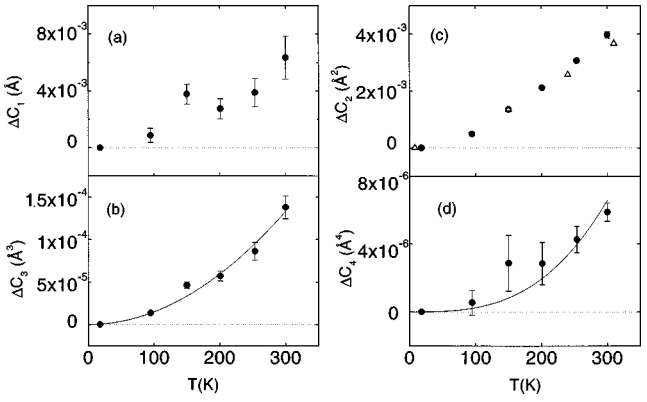

FIG. 5. First four cumulants of the effective distribution of the first-shell Se-Cd distances in CdSe obtained from the analysis of EXAFS phase differences and logarithm of amplitude ratios (full dots). The values of the cumulants are relative to the 18-K reference. The continuous lines in panels (b) and (d) are parabolic and cubic curves best fitting the temperature dependence of the third and fourth cumulants, respectively. The triangles in the plot of ΔC_2 [panel (c)] are the values obtained by Marcus *et al.* for a bulk CdSe sample with the zinc-blende structure (Ref. 28).

neglecting the fourth cumulant, and this can explain the slight discrepancy with respect to our data. As for the difference between zinc blende and wurtzite structure, in the case of AgI the same values of the second cumulant were found for the two structures, within the experimental uncertainty.[33]

IV. RESULTS AND DISCUSSION

The EXAFS analysis described in the previous section has given the temperature dependence of the first four cumulants C_i of the *effective* distribution of the first-shell Se-Cd interatomic distances, $P(r,\lambda,T)$. The effective distribution is connected to the *real* distribution $\rho(r,T)$ through

$$P(r,\lambda,T)=\rho(r,T)\exp(-2r/\lambda)/r^2, \tag{2}$$

where λ is the photoelectron mean free path.[6]

Some relevant, although qualitative, information can be drawn from a direct inspection of Fig. 5. All cumulants regularly grow with temperature. In particular, the behavior of the first cumulant C_1 indicates a slight but not negligible thermal expansion of the average value of the effective distribution, while the behavior of the third and fourth cumulants means that the effective distribution progressively deviates from a Gaussian shape.

A more refined quantitative interpretation of the results requires the reconstruction of the effective and real distributions and of their corresponding mean force potentials. To this aim, the *absolute values* of the cumulants are necessary. The derivation of the absolute values from the relative ones is, however, far from trivial; in what follows we will critically use some of the most common procedures.

The first cumulant C_1 defines the *position* of the effective distribution. The actually relevant information related to thermal expansion is already contained within the relative values $\Delta C_1(T)$. The absolute values $C_1(T)$ are necessary only to calculate the zero-order cumulant for normalization purposes, so they have been determined by simply adding to the experimental values $\Delta C_1(T)$ the approximate crystallographic distance $R=2.63$ Å, assumed valid at 18 K. The zero-order cumulant has then been estimated as

$$C_0=-2C_1/\lambda-2\ \ln\ C_1, \tag{3}$$

where a constant realistic value of 8 Å has been assigned to the mean free path λ.

The second, third, and fourth cumulants describe the *shape* of the effective distribution. Their absolute values are then necessary to reconstruct both the effective and real distributions. As a first approximation, we assumed a classical harmonic behavior for the reference spectrum at 18 K, and identified the relative values ΔC_3 and ΔC_4 with the absolute values C_3 and C_4, respectively. The soundness of this choice will be discussed *a posteriori*.

Once the values of the third and fourth cumulants were established, we faced the problem of determining the second cumulant.

A. Mean square relative displacement

The second cumulant C_2 is the variance of the effective distribution and measures the mean square relative displacement (MSRD) of absorber and backscatterer atoms.

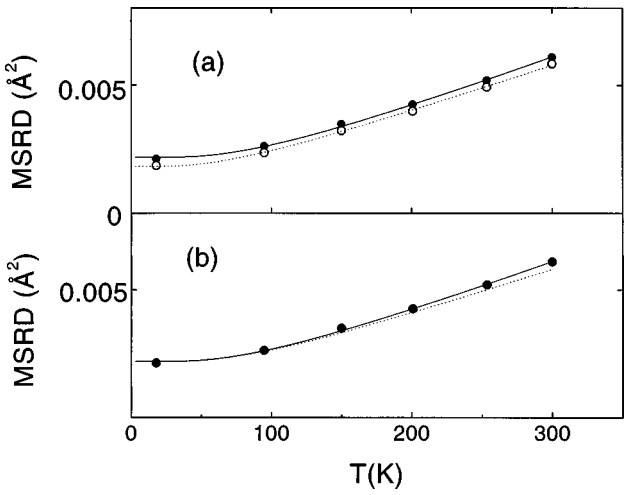

FIG. 6. Absolute values of the MSRD (circles) obtained by fitting a phenomenological model to the slope of the experimental ΔC_2 points. (a) Harmonic correlated Debye (dashed line) and Einstein (continuous line) models; the Einstein model ($\nu_E=4.81$ THz) gives values higher than the Debye model ($q_D=1.28$ Å^{-1}, $\theta=273$ K); the difference is about 8% at 300 K. (b) Einstein model (dotted curve, $\nu_E=4.97$ THz) plus the first-order anharmonic contribution calculated from the experimental cumulants C_3 and C_4; the anharmonic contribution is about 6% of the total MSRD at 300 K.

To get absolute values of C_2 it is customary to fit an Einstein[34] or a Debye correlated model[35] to the slope of experimental ΔC_2 data. In Fig. 6(a) the two models are compared for the first shell of CdSe. The Einstein frequency is $\nu_E=4.81$ THz. The Debye temperature is $\theta_A=273$ K; this value is much larger than the Debye temperature best fitting XRD spectra, $\theta_M=155$ K.[31] A similar difference has been found for other non-Bravais crystals: the EXAFS Debye temperatures θ_A are different for different coordination shells, their values decreasing and approaching the XRD value θ_M when going from the inner to the outer shells.[37] The Debye model gives absolute values of the MSRD slightly lower than the Einstein model; a similar effect was also observed for the first shell of germanium.[37] In general, the Einstein model is preferred for the first shell, on the grounds of both theoretical considerations[36] and experimental verifications.[37]

A refinement of this procedure, which takes into account anharmonicity effects, can be achieved by considering an effective pair potential expanded in power series of the variations u of the interatomic distance with respect to the potential minimum:

$$V_e(u)=au^2/2+bu^3+cu^4+\cdots\ . \tag{4}$$

The cumulants of the effective distributions can be related, in the classical approximation, to the force constants of the potential by the expansion[7,11]

$$\delta C_1=-(3b/a^2)k_BT+\cdots, \tag{5a}$$

$$C_2=(k_BT/a)+(k_BT/a)^2[(6b/a)^2-(12c/a)]+\cdots, \tag{5b}$$

$$C_3=-(k_BT/a)^2(6b/a)+\cdots, \tag{5c}$$

$$C_4=(k_BT/a)^3[(108b^2/a^2)-(24c/a)]+\cdots. \quad (5d)$$

The temperature dependence of the third and fourth cumulants of the Se-Cd distance distribution can actually be fitted by a quadratic and a cubic polynomial, respectively (continuous lines in Fig. 5), as expected from the first-order approximation of Eqs. (5c) and (5d). A more accurate evaluation of the absolute values of the third cumulant, taking into account the low-temperature quantum effects, can be done through Eq. 18 of Ref. 12. However, in the present case of CdSe the difference between classical and quantum treatments is negligible.

In the expression of C_2, Eq. (5b), the first term, representing the harmonic contribution, can be substituted by an Einstein model, $\sigma^2(\omega_E,T)$, which takes into account the zero point energy, and whose frequency is connected to the force constant a by the relation $a=\mu\omega_E^2$. The second term, representing the lowest-order anharmonic contribution, can be expressed as a function of the experimental cumulants C_3 and C_4. The final result is

$$C_2(T)=\sigma^2(\omega_E,T)-\frac{1}{2}\left(\frac{k_BT}{\mu\omega_E^2}\right)^2C_3^2(T)+\frac{1}{2}\left(\frac{k_BT}{\mu\omega_E^2}\right)C_4(T). \quad (6)$$

Equation (6) has only one free parameter, the Einstein frequency. It has been satisfactorily fitted to the slope of the experimental ΔC_2 points, as shown in Fig. 6(b), where the dashed line represents the harmonic contribution, with Einstein frequency $\nu_E=\omega_E/2\pi=4.97$ THz. The anharmonic contribution amounts to about 6% of the total MSRD at 300 K.

This procedure for evaluating and subtracting the anharmonic contribution to the MSRD has been recently applied to the first three coordination shells of germanium.[37,38] Both slope and absolute values of the so obtained harmonic contributions were in good agreement with three different theoretical calculations: a bond charge model, a high temperature expansion of the projected density of vibrational states, and a first-principles approach, respectively.

Sometimes the temperature dependence of the MSRD has been fitted by a $T^{3/2}$ law to account for anharmonicity effects.[28,39] The use of Eq. (6) has the advantage of estimating the anharmonic term directly from the experimental cumulants; besides, it allows a reliable estimate of the absolute values of the MSRD.

B. Effective distribution and mean force potential

Once the absolute values of the leading cumulants have been established, it is possible to reconstruct the effective distributions of distances $P(r,\lambda,T)$.[8] To this purpose, the following procedure has been adopted.

Complex characteristic functions have been calculated, for all the temperatures considered, as

$$\Psi(2k)=\exp\left[\sum_{n=0}^{n=4}\frac{(2ik)^n}{n!}C_n\right] \quad (7)$$

within a k range extending from -35 to $+35$ Å^{-1} [Fig. 7(a)]. The choice of the maximum value of $|k|$, larger than the experimental value $k_{max}=15$ Å^{-1}, was made on the assumption that the cumulants of order higher than 4 were negligible up to 35 Å^{-1}, so that the EXAFS signal could be extrapolated not only down to $k=0$ Å^{-1}, but also up to $k=35$ Å^{-1}. Actually, the characteristic function was regularly damped at the boundaries even at 300 K, and no windowing was necessary before Fourier transforming. A similar procedure was utilized for amorphous germanium thin films;[40] in that case the distribution of distances reconstructed from EXAFS cumulants was in good agreement with the one determined by Filipponi and DiCicco[41] through a completely different EXAFS analysis based on theoretical calculation of phase shifts and amplitudes and taking into account spherical wave effects.

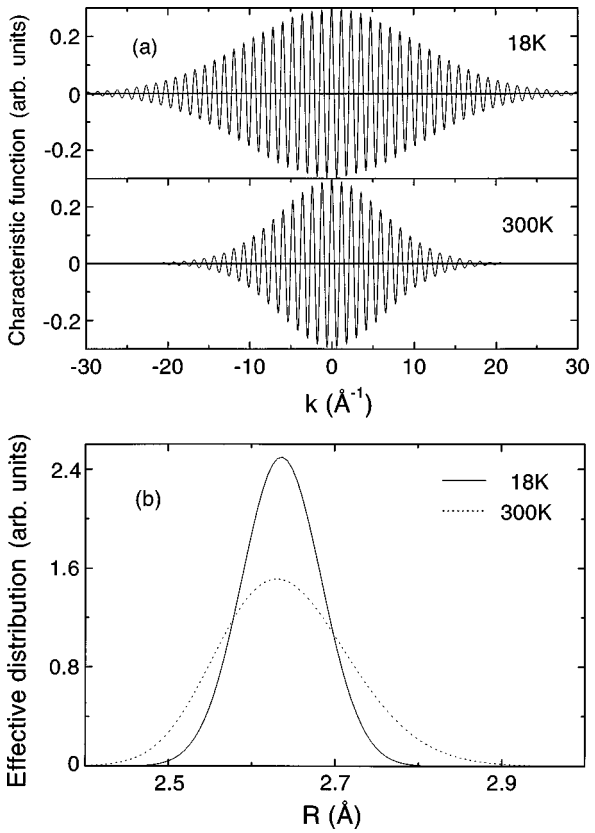

FIG. 7. Characteristic functions (a) and effective distributions of interatomic distances (b) reconstructed from the EXAFS cumulants at 18 and 300 K.

The real part of the complex Fourier transform of the characteristic function Eq. (7) is the effective distribution of distances $P(r,\lambda,T)$ [Fig. 7(b)]; the imaginary part of the Fourier transform is identically zero. Both the average value and the asymmetry of the effective distribution increase with temperature, in connection with the growth of the first and third cumulants. The position of the maximum of the distribution decreases when the temperature increases.

In the classical approximation the effective distribution of distances can be expressed as a canonical average

$$P(r,\lambda,T)=\frac{e^{-V(r)/kT}}{\int e^{-V(r)/kT}dr}, \quad (8)$$

where $V(r)$ is a *mean force pair potential*,[42] which depends on the statistically averaged behavior of all the atoms in the

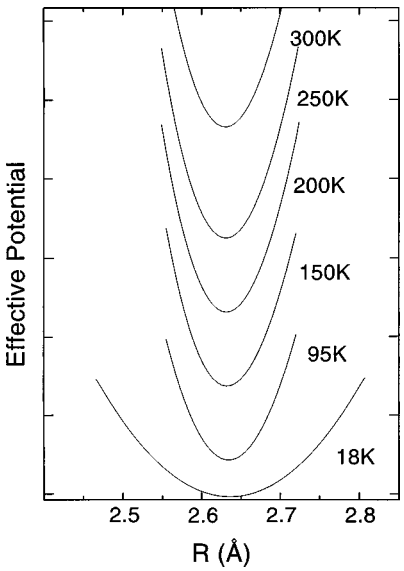

FIG. 8. Mean force potentials calculated in classical approximation from the effective distributions reconstructed from EXAFS cumulants. The curves at each temperature have been vertically shifted for clarity.

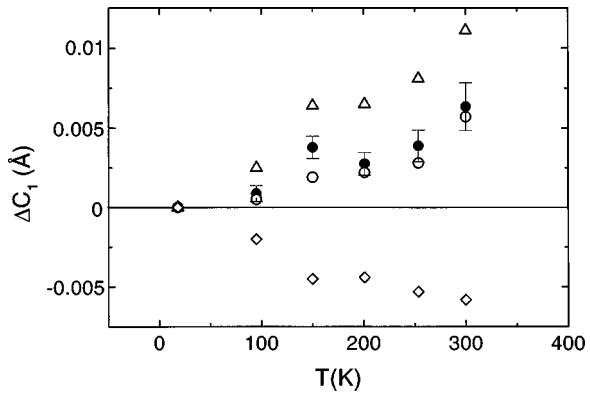

FIG. 9. Effective distribution of distances in CdSe: comparison between the first cumulant ΔC_1 (full circles), the ratio $C_3/2C_2$ (triangles), and the shift of the minimum of the mean force potential (diamonds). The open circles have been obtained by adding the values $C_3/2C_2$ to the potential shifts.

crystal.[21] We stress that the potential considered here and in the previous paper on AgI (Ref. 10) depends on the scalar distance r like the effective distribution, while in Ref. 22 a potential $V(\vec{r})$ is considered, depending on the vector position $\vec{r}$.

The mean force pair potentials $V(r)$ for the first shell of CdSe have been obtained from the effective distributions at different temperatures by inverting Eq. (8), and are shown in Fig. 8. Below 150 K the shape of the potentials depends on temperature, reflecting the inadequacy of the classical approximation underlying Eq. (8); however, above 150 K the shape of the potentials is nearly independent of temperature, indicating the soundness of the classical approximation. The relatively low temperature at which the classical approximation is still valid is connected to the low Einstein frequency of the MSRD and explains why there is no significant difference between the quantum and classical behavior of the third cumulant.

The position of the minimum of the potential $V(r)$, corresponding to the maximum of the distribution, shifts toward lower values when the temperature increases. A similar effect was found for AgI in the temperature range from 150 to 370 K (Ref. 10); in that case the same shift characterized the effective distributions and mean force potentials obtained not only from EXAFS spectra but also from a molecular-dynamics simulation based on the pair potentials optimized by Parrinello *et al.*[43]

The temperature dependence of the minimum of the potential does not depend on the inadequacy of the classical approximation, but reflects an intrinsic characteristic of the mean force pair potential in crystals. The results obtained from single-bond potentials[12] cannot be directly applied to crystals.

Equations (5a)–(5d) express the temperature dependence of the first four cumulants as expected in the classical approximation for a potential independent of temperature. In particular, to first order $\delta C_1 = C_3/2C_2$. This relation has been sometimes utilized to estimate the thermal expansion from the values of the second and third cumulants.[9] We want to stress the difference between the values ΔC_1, directly measured from EXAFS phases [Fig. 5(a)] and the values δC_1 of Eq. (5a). ΔC_1 is the actual variation of the average value of the effective distribution, and depends on both the shape and the position of the mean force potential $V(r)$, while δC_1 only depends on the shape of the mean force potential. The difference is clearly depicted for CdSe in Fig. 9, where the triangles are the values $C_3/2C_2$, corresponding to δC_1, the full circles are the values ΔC_1 (notice that the experimental values C_2 utilized to calculate the ratio $C_3/2C_2$ have the correct low-T quantum behavior). The diamonds in Fig. 9 represent the shift of the position of the minimum of the potential. The values ΔC_1 are in good agreement with the sum of the $C_3/2C_2$ values and the potential shift (open circles). Similar results had been previously found for AgI, although with a higher degree of experimental uncertainty.[10]

The temperature dependence of the position of the mean force potential does not invalidate the procedure followed for calculating the absolute values of C_2, based on a constant potential, Eq. (4). Actually in Eq. (6) only the shape of the potential is involved, not the position.

C. Thermal expansion

The thermal expansion measured by EXAFS is the variation with temperature of the average position C_1^* of the real distribution of distances. The relation between the first cumulants of the effective and real distributions of distances, C_1 and C_1^*, respectively, is well established[5,44] and can be expressed as

$$C_1 = C_1^* - \frac{2C_2^*}{C_1^*}\left(1 + \frac{C_1^*}{\lambda}\right). \tag{9}$$

The second cumulants of the effective and real distributions are generally considered equal and, for crystalline solids, expressed to a good approximation as $C_2 = C_2^* = \langle(\Delta u_\parallel)^2\rangle$. Here $\Delta u_\parallel = \hat{R}\cdot(\vec{u}_j - \vec{u}_0)$ is the *radial* component of the relative instantaneous displacement $\vec{u}_j$ and $\vec{u}_0$ of the

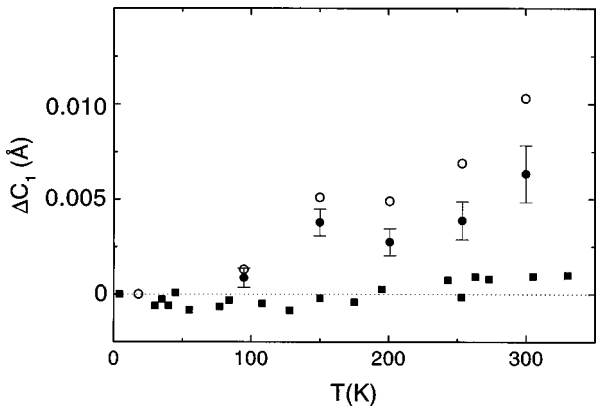

FIG. 10. Temperature dependence of the first-shell interatomic distance in CdSe measured by XRD and EXAFS. The squares are the ΔR values from XRD. The full and open circles are the values ΔC_1 and ΔC_1^* for the effective and real distributions, respectively, determined from EXAFS.

backscatterer and absorber atoms, respectively.[35] The angular brackets indicate a canonical average.

In Fig. 10 the temperature dependence of the first cumulant of the effective distribution (full circles) is compared with the temperature dependence of the first cumulant of the real distribution (open circles), calculated through Eq. (9). The difference $\Delta C_1^* - \Delta C_1$ amounts to about 0.004 Å at 300 K.

Also shown in Fig. 10 is the first-shell thermal expansion ΔR calculated from XRD measurements (squares).[25] The thermal expansion measured by EXAFS is very large as compared with the one measured by XRD. The difference $\Delta C_1^* - \Delta R$ amounts to 0.011 Å at 300 K. A similar behavior was found for β-AgI, which has the same wurtzite structure as CdSe.[10]

The discrepancy between EXAFS and XRD can be explained on the grounds of the following considerations. The relation between the average value C_1^* of the real distribution and the distance R between the centers of thermal ellipsoids of absorber and backscatterer atoms can be expressed as a function of the thermal atomic displacements:[45–47]

$$C_1^* = R + \frac{\langle (\Delta u_\perp)^2 \rangle}{2R}. \tag{10}$$

Here $\Delta u_\perp$ is the *transverse* component of the relative atomic instantaneous displacement: $(\Delta u_\perp)^2 = (\Delta u)^2 - (\Delta u_\parallel)^2$. According to Eq. (10), C_1^* is larger than R owing to the effect of thermal vibrations normal to the bond direction. Since $\langle (\Delta u_\perp)^2 \rangle$ grows with temperature, the thermal expansion measured by EXAFS is larger than the real one; an apparent thermal expansion should be observed by EXAFS also for a perfectly harmonic crystal.

To recover the true thermal expansion from EXAFS data one should know the value of $\langle (\Delta u_\perp)^2 \rangle$. Like the MSRD $\langle (\Delta u_\parallel)^2 \rangle$, also $\langle (\Delta u_\perp)^2 \rangle$ is sensitive to the correlation of vibrational motion of absorber and backscatterer atoms. If the correlations in the radial and transverse directions were equal, the ratio $\gamma = \langle (\Delta u_\perp)^2 \rangle / \langle (\Delta u_\parallel)^2 \rangle$ would be equal to 2, and the term $\langle (\Delta u_\perp)^2 \rangle$ could be directly obtained from the measurement of the second cumulant $C_2 = \langle (\Delta u_\parallel)^2 \rangle$. A ratio $\gamma = 2$ was assumed in Refs. 2, 19, and 23.

However, the correlation function is generally different in the radial and transverse directions, so the evaluation of $\langle (\Delta u_\perp)^2 \rangle$ directly from EXAFS data is not possible. As a matter of fact, the present EXAFS results for CdSe are consistent with the XRD thermal expansion if one assumes a γ ratio about equal to 13. In the case of β-AgI, which has the same wurtzite structure, a ratio $\gamma \simeq 10$ was experimentally found.[10] Theoretical calculations for germanium, based on a bond charge model,[48] led to a ratio γ for the first coordination shell growing from about 3.3 at 100 K to about 5 at 300 K.

The effect of thermal vibrations normal to the bond direction could explain, at least qualitatively, the difference found by Marcus *et al.*[28] between the interatomic distances determined by EXAFS and XRD in CdSe nanoparticles. The absence of contraction in EXAFS data could be due to the influence of strong vibrations of surface atoms in directions parallel to the surface (normal to the bonds with inner atoms).

Since the first temperature-dependent EXAFS studies, it had been pointed out that the reproduction of the EXAFS MSRD was an original test for vibrational dynamics calculations, since the MSRD carries peculiar information on the correlation *parallel* to the bond direction.[34,35] The present work shows that the comparison between thermal expansion measured by EXAFS and XRD allows one to determine the ratio $\gamma = \langle (\Delta u_\perp)^2 \rangle / \langle (\Delta u_\parallel)^2 \rangle$, which contains information on the correlation *normal* to the bond direction, and represents then a new independent test of vibrational calculations.

The anharmonicity of the mean force potential sampled by EXAFS not only depends on the real crystal anharmonicity, which is responsible for the true XRD thermal expansion, but is also enhanced by the effect of thermal vibrations normal to the bond direction. This opens new questions about the meaning of the high-order cumulants. In particular, the third cumulant C_3, which measures the asymmetry of the distribution and is related to thermal expansion, could depend on thermal vibrations normal to the bond direction; in that case, as an effect of the zero point thermal motion, it should not be zero at zero K also in the classical approximation, and the determination of its absolute values from the experimental relative values should be far from trivial.

V. CONCLUSIONS

The high quality of the EXAFS spectra of bulk CdSe has allowed a very accurate determination of the cumulants of the first shell in the temperature range from 18 to 300 K. The anharmonicity effects are well evident and not negligible even at relatively low temperatures.

The effective distributions of the first-shell Cd-Se inter atomic distances and the corresponding mean force potentials have been reconstructed at various temperatures. The mean force pair potential $V(r)$ is temperature dependent in both shape and position: however, while the variations in shape depend on the drawbacks of the classical approximations and are negligible above 150 K, the shift of the minimum position is regular in all the temperature range; the EXAFS cumulants in crystals cannot be connected to a con-

stant anharmonic pair potential. As a consequence, the variation of the average value C_1 of the distribution depends both on the position and on the shape of the potential, so that ΔC_1 is not equivalent to $C_3/2C_2$.

The interatomic distance measured by EXAFS is larger than the distance betwen the centers of thermal ellispoids, as determined by XRD, owing to the effect of thermal vibrations normal to the bond direction. Correspondingly, EXAFS measures a thermal expansion artificially larger than the true one. In order to recover the true thermal expansion from EXAFS spectra one should know the eigenfrequencies and eigenvectors of the dynamical matrix. Conversely, the comparison between EXAFS and XRD thermal expansion can give original information on the correlation of vibrational motion normal to the bond direction, say on phase relationships between eigenvectors.

The very meaning of the anharmonicity of the mean force potential sampled by EXAFS should be questioned. Actually, the EXAFS potential reflects not only the anharmonicity of the crystal potential, which is responsible for the true thermal expansion, but also the anharmonicity created as an effect of the correlation of vibrational motion normal to bond direction. As a consequence, also the meaning of the high-order EXAFS cumulants should be reexamined.

ACKNOWLEDGMENTS

The collaboration of F. Rocca and C. Armellini (CNR-ITC, Trento) in preparing and XRD characterizing the sample, and the help of A. Traverse and F. Villain (LURE, Orsay) during synchrotron radiation measurements are acknowledged. This work has been partially funded by the EC program Training and Mobility of Researchers for Large Scale Facilities. One of the authors (D.D.) is grateful to the Swedish Agency for Research Cooperation with Developing Countries (SAREC) and the International Centre for Theoretical Physics (ICTP, Trieste) for financial support. D.D. is a Regular Associate of ICTP, Trieste, Italy.

[1] P. A. Lee, P. H. Citrin, P. Eisenberger, and B. M. Kincaid, Rev. Mod. Phys. **53**, 769 (1981).
[2] P. Eisenberger and G. S. Brown, Solid State Commun. **29**, 481 (1978).
[3] T. M. Hayes, J. B. Boyce, and J. L. Beeby, J. Phys. C **11**, 2931 (1978).
[4] E. D. Crozier and A. Seary, Can. J. Phys. **58**, 1388 (1980).
[5] G. Bunker, Nucl. Instrum. Methods Phys. Res. **207**, 437 (1983).
[6] E. D. Crozier, J. J. Rehr, and R. Ingalls, in *X-Ray Absorption*, edited by D. C. Koningsberger and R. Prins (Wiley, New York, 1988).
[7] J. M. Tranquada and R. Ingalls, Phys. Rev. B **28**, 3520 (1983).
[8] E. A. Stern, Y. Ma, O. Hanske-Petitpierre, and C. Bouldin, Phys. Rev. B **46**, 687 (1992).
[9] L. Tröger, T. Yokoyama, D. Arvanitis, T. Lederer, M. Tischer, and K. Baberschke, Phys. Rev. B **49**, 888 (1994).
[10] G. Dalba, P. Fornasini, R. Gotter, and F. Rocca, Phys. Rev. B **52**, 149 (1995).
[11] E. A. Stern, P. Livins, and Z. Zhang, Phys. Rev. B **43**, 8850 (1991).
[12] A. I. Frenkel and J. J. Rehr, Phys. Rev. B **48**, 585 (1993).
[13] T. Yokoyama, K. Kobayashi, T. Ohta, and A. Ugawa, Phys. Rev. B **53**, 6111 (1996).
[14] T. Yokoyama, Y. Yonamoto, T. Ohta, and A. Ugawa, Phys. Rev. B **54**, 6921 (1996).
[15] T. Yokoyama, K. Kobayashi, and T. Ohta, J. Phys. Soc. Jpn. **65**, 3901 (1996).
[16] T. Fujikawa and T. Miyanaga, J. Phys. Soc. Jpn. **62**, 4108 (1993).
[17] T. Miyanaga and T. Fujikawa, J. Phys. Soc. Jpn. **63**, 1036 (1994).
[18] T. Miyanaga and T. Fujikawa, J. Phys. Soc. Jpn. **63**, 3683 (1994).
[19] T. Ishii, J. Phys.: Condens. Matter **4**, 8029 (1992).
[20] O. Kamishima, T. Ishii, H. Maeda, and S. Kashino, Solid State Commun. **103**, 141 (1997).
[21] J. Mustre de Leon, S. D. Conradson, I. Batistić, A. R. Bishop, I. D. Raistrick, M. C. Aronson, and F. H. Garzon, Phys. Rev. B **45**, 2447 (1992).
[22] E. A. Stern, J. Phys. IV **7**, C2-137 (1997).
[23] T. Yokoyama, T. Ohta, and H. Sato, Phys. Rev. B **55**, 11 320 (1997).
[24] N. Van Hung and J. J. Rehr, Phys. Rev. B **56**, 43 (1997).
[25] Y. S. Touloukian, R. K. Kirby, R. E. Taylor, and P. D. Desai, *Thermophysical Properties of Matter* (Plenum, New York, 1977), Vol. 13.
[26] M. G. Bawendi, A. R. Kortan, M. L. Steigerwald, and L. E. Brus, J. Chem. Phys. **91**, 7282 (1989).
[27] M. A. Marcus, L. E. Brus, C. Murray, M. G. Bawendi, A. Prasad, and A. P. Alivisatos, Nanostruct. Mater. **1**, 323 (1992).
[28] M. A. Marcus, W. Flood, M. Stiegerwald, L. Brus, and M. Bawendi, J. Phys. Chem. **95**, 1572 (1991).
[29] A. Demourgues, G. N. Greaves, R. Bilsborrow, G. Baker, A. Sery, A. J. Dent, and B. Speit, Physica B **208&209**, 354 (1995).
[30] G. Dalba, D. Diop, P. Fornasini, R. Grisenti, D. Pasqualini, F. Rocca, and A. Traverse, J. Phys. IV **7**, C2-237 (1997).
[31] A. W. Stevenson and Z. Barnea, Acta Crystallogr., Sect. B: Struct. Sci. **40**, 530 (1984).
[32] G. Dalba, P. Fornasini, and F. Rocca, Phys. Rev. B **47**, 8502 (1993).
[33] G. Dalba, P. Fornasini, and F. Rocca, J. Phys.: Condens. Matter **4**, 1121 (1992).
[34] E. Sevillano, H. Meuth, and J. J. Rehr, Phys. Rev. B **20**, 4908 (1979).
[35] G. Beni and P. M. Platzman, Phys. Rev. B **14**, 1514 (1976).
[36] E. A. Stern, in *X-Ray Absorption*, edited by D. C. Koningsberger and R. Prins (Wiley, New York, 1988).
[37] G. Dalba and P. Fornasini, J. Synchrotron Radiat. **4**, 243 (1997).
[38] G. Dalba, P. Fornasini, M. Grazioli, and F. Rocca, Phys. Rev. B **52**, 11 034 (1995).
[39] M. Marcus and C. L. Tsai, Solid State Commun. **52**, 511 (1984).
[40] G. Dalba, P. Fornasini, R. Grisenti, F. Rocca, I. Chambouleyron, and C. F. O. Graeff, J. Phys.: Condens. Matter **9**, 5875 (1997).
[41] A. Filipponi and A. DiCicco, Phys. Rev. B **51**, 12 322 (1995).
[42] N. E. Cusack, *The Physics of Structurally Disordered Matter* (Adam Hilger, Bristol, 1987).
[43] M. Parrinello, A. Rahman, and P. Vashishta, Phys. Rev. Lett. **50**, 1073 (1983).

[44] J. Freund, R. Ingalls, and E. D. Crozier, Phys. Rev. B **39**, 12 537 (1989).
[45] W. R. Busing and H. R. Levy, Acta Crystallogr. **17**, 142 (1963).
[46] B. T. M. Willis and A. W. Pryor, *Thermal Vibrations in Crystallography* (Cambridge University Press, Cambridge, England, 1975).
[47] P. Lagarde, in *Amorphous Solids and the Liquid State*, edited by N. H. March, R. A. Street, and M. Tosi (Plenum Press, New York, 1985), p. 365.
[48] O. H. Nielsen and W. Weber, J. Phys. C **13**, 2449 (1980).